Valence-bond insulator in proximity to excitonic instability

Y. Chiba, T. Mitsuoka, N. L. Saini, K. Horiba, M. Kobayashi, K. Ono, H. Kumigashira, N. Katayama, H. Sawa, M. Nohara, Y. F. Lu, H. Takagi, and T. Mizokawa

Phys. Rev. B **100**, 245129 — Published 18 December 2019

DOI: 10.1103/PhysRevB.100.245129

A valence-bond insulator in proximity to excitonic instability

Y. Chiba,[1] T. Mitsuoka,[2] N. L. Saini,[3] K. Horiba,[4] M. Kobayashi,[4] K. Ono,[4] H. Kumigashira,[4] N. Katayama,[5] H. Sawa,[5] M. Nohara,[6] Y. F. Lu,[7] H. Takagi,[8,7] and T. Mizokawa[2]

[1]*Department of Physics, University of Tokyo, 5-1-5 Kashiwanoha, Chiba 277-8561, Japan*

[2]*Department of Applied Physics, Waseda University, Shinjuku, Tokyo 169-8555, Japan*

[3]*Department of Physics, University of Roma "La Sapienza" Piazalle Aldo Moro 2, 00185 Roma, Italy*

[4]*Institute of Materials Structure Science, High Energy Accelerator Research Organization (KEK), Tsukuba, Ibaraki 305-0801, Japan*

[5]*Department of Applied Physics, Nagoya University, Nagoya 464-8603, Japan*

[6]*Research Institute for Interdisciplinary Science, Okayama University, Okayama 700-8530, Japan*

[7]*Department of Physics, University of Tokyo, Tokyo 113-0033, Japan*

[8]*Max Planck Institute for Solid State Research, 70569 Stuttgart, Germany*

(Dated: December 2, 2019)

Abstract

Ta_2NiS_5 is supposed to be a simple semiconductor in which excitonic instability of Ta_2NiSe_5 is suppressed due to its large band gap. However, the Ni $2p$ core-level photoemission of Ta_2NiS_5 exhibits a satellite indicating Ni $3d$ orbitals are mixed into its conduction band as expected in an excitonic insulator. The valence band does not show dispersion flattening and spectral sharpening which are fingerprints of excitonic insulator. Instead, Ni $3p$-$3d$ resonant photoemission indicates Mottness of the Ni $3d$ electron in Ta_2NiS_5 with negative charge-transfer energy. The present results show that Ta_2NiS_5 can be viewed as a valence bond insulator with a band gap exceeding the exciton binding energy.

PACS numbers: 71.35.Lk, 71.20.-b, 67.85.Jk, 03.75.Nt

I. INTRODUCTION

Semimetals with hole and electron Fermi pockets or semiconductors with a narrow band gap tend to exhibit charge-spin-orbital density wave transitions due to electronic coupling between the Fermi surfaces or between the valence band top and the conduction band bottom. Such charge-spin-orbital instabilities can be described by the theoretical framework of the excitonic insulator which has been established in 1960's[1–4]. When the exciton binding energy between the hole and electron is larger than the magnitude of the band gap, the semiconductor or semimetal ground state undergoes the coherent formation of excitons which corresponds to the transition to the charge-spin-orbital density waves.

As for candidates of excitonic insulator, Tm(Se,Te) has been proposed to be an excitonic insulator under pressure[5–7] although it is not established yet due to difficulty of spectroscopic study under pressure. Another candidate $1T$-$TiSe_2$[8] has been studied by means of angle-resolved photoemission spectroscopy (ARPES)[9–16] as well as time-resolved ARPES[17] and electron energy loss spectroscopy[18]. Although the spectroscopic studies on $1T$-$TiSe_2$ have suggested the excitonic coupling between the valence band top and the conduction band bottom, it is still controversial whether the transition of $1T$-$TiSe_2$ is driven by excitonic coupling or electron-lattice coupling. In addition, effect of excitonic coupling has been discussed in strongly correlated transition-metal oxides such as $Pr_{0.5}Ca_{0.5}CoO_3$[19] and Ca_2RuO_4[20] in which the interplay between Mottness and excitonic coupling may create novel quantum states.

Among the excitonic insulator candidates, Ta_2NiSe_5 is very unique in that it is semiconducting below and above the transition temperature[21,22]. In addition, the transition is accompanied by a very small lattice distortion in contrast to the large distortion in $1T$-$TiSe_2$. Therefore, Ta_2NiSe_5 is likely to be the most promising candidate located in the semiconducting side of the excitonic insulator phase diagram. Actually, ARPES studies on Ta_2NiSe_5 suggest the BEC type transition[23,24], which is consistent with the theoretical calculations on a realistic model[25–27]. On the other hand, semiconducting Ta_2NiS_5 does not show any transitions probably due to the relatively large band gap as demonstrated by the recent transport and optical studies[28–30]. In Ta_2NiSe_5, ultrafast optical response of the excitonic order parameter has been extensively studied by pump-probe reflectivity experiment[31,32] and time-resolved ARPES[33,34]. In Ta_2NiS_5, the exciton binding energy is smaller than the band

gap and the excitonic instability can be suppressed[29]. However, a time-resolved ARPES study has revealed that the band gap of Ta_2NiS_5 collapses by optical excitation in a similar manner to Ta_2NiSe_5[34]. Therefore, although Ta_2NiS_5 does not show any phase transitions, its electronic structure may deviate from that of conventional band insulators. In this context, it is very interesting to study the electronic structure of Ta_2NiS_5 and compare it with that of Ta_2NiSe_5.

II. EXPERIMENT

Single crystals of Ta_2NiS_5 were grown as reported in the literatures[28]. The single crystals were cleaved *in situ* for XPS and ARPES measurements. XPS was performed at room temperature using a JPS9200 analyzer equipped with a monochromatized Mg $K\alpha$ line ($h\nu =$ 1253.6 eV) as a light source with an energy resolution of ~ 0.6 eV. The ARPES measurements were performed at beamline 28A of Photon Factory, KEK using a SCIENTA SES-2002 electron analyzer with circularly polarized light. The total energy resolution was set to 20 - 30 meV for the excitation energies from $h\nu = 41$ - 67 eV. The base pressure of the spectrometer was in the 10^{-9} Pa range. The single crystals oriented by *ex situ* Laue diffraction, were cleaved at 200 K under the ultrahigh vacuum and the spectra were acquired at various temperatures. The Fermi level (E_F) was determined using the Fermi edge of gold reference samples.

III. RESULTS AND DISCUSSION

The orthorhombic crystal structure of Ta_2NiS_5 is illustrated in Fig. 1(a). The Ni chain and Ta double chain run along the a-axis. The cleavage surface corresponds to the ac-plane. Possible electronic configurations for Ni $3d$ and Ta $5d$ and one eighth of the Brillouin zone are also illustrated in Fig. 1(a). Figure 1(b) shows the band dispersions of the entire valence band for Ta_2NiS_5. The valence band exhibits substantial dispersions along the a-axis (chain direction) corresponding to the Z-U or T-R direction in the Brillouin zone. On the other hand, the band dispersions along the Z-Γ or T-Y direction are relatively small in consistent with the ARPES results for Ta_2NiSe_5[23,24]. In addition, the band dispersions are negligibly small along the Z-T direction which is perpendicular to the cleaved surface.

Figure 2 shows the Ni $2p$ core-level XPS spectra of Ta_2NiSe_5 and Ta_2NiS_5. Both Ta_2NiSe_5 and Ta_2NiS_5 exhibit the satellite structure located at binding energy of $\sim$ 861 eV. The satellite structure can be reproduced by the NiS_4 or $NiSe_4$ cluster model calculation. The calculated result with U = 3.0 eV, $\Delta = -2.5$ eV, and $(pd\sigma) = -2.2$ eV is indicated by the solid curve in Fig. 2. The agreement between the calculation and the experimental results is reasonably good, indicating that both Ta_2NiSe_5 and Ta_2NiS_5 have the negative Δ. Here U, Δ, $(pd\sigma)$ are the multiplet-averaged d-d Coulomb interaction energy, the Se $4p$(S $3p$)-to-Ni $3d$ charge transfer energy, and the transfer integral written in the Slater-Koster manner[36–38]. In the present cluster model, the Coulomb interaction between the Ni $3d$ electrons are given by the Slater integrals $F^0(3d, 3d)$, $F^2(3d, 3d)$, and $F^4(3d, 3d)$. The average Ni $3d$-Ni $3d$ Coulomb interaction U is expressed by $F^0(3d, 3d)$ and is an adjustable parameter. $F^2(3d, 3d)$ and $F^4(3d, 3d)$ are fixed to 80% of the atomic Hartree-Fock values[39]. The Coulomb interaction between the Ni $2p$ core hole and the Ni $3d$ electron is expressed by the Slater integrals $F^0(2p, 3d)$, $F^2(2p, 3d)$, and $G^1(2p, 3d)$. The average Ni $2p$-Ni $3d$ Coulomb interaction Q is expressed by $F^0(2p, 3d)$ and is fixed to $U/0.8$. $F^2(2p, 3d)$ and $G^1(2p, 3d)$ are fixed to 80% of the atomic Hartree-Fock values[39]. The ground state with $^3T_2$ symmetry is given by a linear combination of d^8, d^9L, and $d^{10}L^2$ configurations where L denotes a ligand hole in the S $3p$ or Se $4p$ orbital. The final states are given by linear combinations of cd^8, cd^9L, and $cd^{10}L^2$ configurations where c denotes a Ni $2p$ core hole. The negative charge transfer energy $\Delta = -2.5$ eV shows that the ground states are dominated by d^9L rather than d^8 and that holes are already located at the itinerant S $3p$ or Se $4p$ orbitals in the ground state.

The existence of the charge transfer satellite has encouraged us to perform Ni $3p$-$3d$ resonant photoemission measurement. Figures 3 shows the Ni $3p$-$3d$ resonant photoemission spectra for Ta_2NiSe_5 and Ta_2NiS_5. The intensity of the satellite region around $\sim$ -5 eV below E_F depends on the incident photon energy indicating the interference between the $3d^9L \rightarrow 3d^8L + \epsilon$ process and the $3d^9L \rightarrow c3d^{10}L \rightarrow 3d^8L + \epsilon$ process. Here, c denotes a Ni $3p$ core hole. The resonance behavior is somewhat similar to that reported for NiS_2 with small charge transfer energy[40]. The enhancement of the satellite at the resonance ($h\nu = 65$ eV) is stronger in Ta_2NiS_5 than in Ta_2NiSe_5. As shown in the insets of Fig. 3, the intensity of the satellite is enhanced by $\sim$ 80% in going from $h\nu = 57$ eV to 65 eV forTa_2NiS_5 while it is enhanced by $\sim$ 20% forTa_2NiSe_5. In addition, the resonance behavior of the main valence

band at $\sim$ -2 eV is much more significant in Ta_2NiS_5 than in Ta_2NiSe_5. In Ta_2NiS_5, the small spectral weight around -0.2 eV observed at $h\nu = 57$ eV can be assigned to a surface state formed within the band gap.

The unoccupied part of the Ni $3d$ and S $3p$ orbitals indicated by the Ni $2p$ XPS for Ta_2NiS_5 would be consistent with the excitonic coupling between the Ni $3d$ - S $3p$ valence band and the Ta $5d$ conduction band. However, the unoccupied Ni $3d$ or S $3p$ level is not sufficient to have an excitonic insulator transition. Since the band gap of Ta_2NiS_5 is larger than the excitonic binding energy, the excitonic instability is expected to be suppressed. As for Ta_2NiSe_5, since the Ni $3d$ - Se $4p$ state is coupled to the Ta $5d$ state, the excited Ni $3d$ - Se $4p$ electron is quickly escaped from the Ni $3p$ core hole site to the Ta $5d$ site to suppress the resonance. In this situation, the Ni $3p$ core hole tends to decay by the normal Auger process. Indeed, the Auger peak is clearly observed in Ta_2NiSe_5 as shown in Fig. 3(b). On the other hand, in Ta_2NiS_5 without the excitonic coupling, the excited Ni $3d$ - S $3p$ electron remains at the Ni $3p$ core hole site and provides the Ni $3p$-$3d$ resonance behavior. The strong resonance behavior is derived from Mottness of Ni $3d$ indicating that Ta_2NiS_5 is a valence bond insulator with localized Ni $3d$ and S $3p$ holes.

The next question is why Ta_2NiS_5 can have the substantial band gap in spite of the unoccupied Ni $3d$ orbitals similar to Ta_2NiSe_5. When the Ni $3d$ orbitals are partially occupied and the charge transfer energy is positive, the system becomes a charge transfer type Mott insulator such as CuO[36,37]. On the other hand, the system with negative charge transfer energy can be described as a valence bond insulator just like $NaCuO_2$[41]. Therefore, in Ta_2NiS_5, the S $3p$ ligand hole is strongly tied to the Ni $3d$ hole forming the spin singlet state. The substantial band gap is formed by the local hybridization between the Ni $3d$ and S $3p$ orbitals exceeding the exciton binding energy.

Figures 4(a) and (b) show the ARPES spectra of the valence band around the Z point of the Brillouin zone for Ta_2NiSe_5 and Ta_2NiS_5 taken at 200 K, respectively. Since the exciton binding energy of about 0.3 eV is smaller than the band gap of Ta_2NiS_5[29], the excitonic insulator transition is expected to be suppressed. Figures 4(c) and (d) show the valence band ARPES spectra of Ta_2NiSe_5 and Ta_2NiS_5 taken at 40 K, where the dispersion flattening and spectral sharpening are clearly seen in Ta_2NiSe_5 consistent with the previous studies[23,24]. On the other band, the valence band dispersion does not show any appreciable change in Ta_2NiS_5.

The satellite structure in the Ni $2p$ photoemission spectra indicates the $3d^9L$ character both in Ta_2NiSe_5 and Ta_2NiS_5 where L represents a ligand hole. In the simplified picture, the difference between Ta_2NiSe_5 and Ta_2NiS_5 depends on whether the ligand hole is tied to the Ni site or the Ta site. In case of Ta_2NiS_5, the ligand hole is confined in the NiS_4 cluster, and the system becomes a valence bond insulator where the Ni 3d spins and ligand holes form a spin singlet and obtains a band gap larger than the exciton binding energy. On the other hand, in Ta_2NiSe_5, since the ligand hole is not confined in the $NiSe_4$ cluster, the band gap becomes smaller than the exciton binding energy and the system exhibits the excitonic instability. The proximity between the valence bond insulator and the excitonic insulator suggests that transition-metal compounds with negative charge transfer energy with $d^{n+1}L$ ground state may have instability towards excitonic insulators. It would be interesting to explore high valence transition-metal oxides or transition-metal chalcogenides along this line as possible candidates of excitonic insulators.

IV. CONCLUSION

In summary, we have investigated the electronic structure of Ta_2NiS_5 by means of Ni $2p$ x-ray photoemission, Ni $3p$-$3d$ resonant photoemission, and angle-resolved photoemission spectroscopy. In the Ni $2p$ core-level spectra, Ta_2NiS_5 and Ta_2NiSe_5 commonly exhibit charge transfer satellites, indicating that the Ni $3d$ subshell is partly unoccupied and that the S $3p$ or Se $4p$ orbitals accommodate holes. The Ni $3p$-$3d$ resonance spectra indicate that the S $3p$ hole is bounded to the Ni site in Ta_2NiS_5 while the Se $4p$ hole is more itinerant in Ta_2NiSe_5. The dispersion flattening and spectral sharpening of the valence band are observed only in Ta_2NiSe_5, and the excitonic instability is suppressed in Ta_2NiS_5. Ta_2NiS_5 can be viewed as a valence bond insulator in which the band gap is formed due to hybridization between localized Ni $3d$ electrons and S $3p$ holes. The present work suggests that the transition-metal compounds with small or negative charge-transfer energies may commonly show excitonic instability if the coupling between the transition-metal d electron and the ligand p hole can be modified by chemical effect or external stimuli.

Acknowledgement

The authors would like to thank Prof. H. Fukuyama, Prof. Y. Ohta, and Prof. C. Monney for the valuable discussions and Dr. Y. Wakisaka and Dr. D. Ootsuki for the contributions at the early stage of this work. This work was partially supported by Grants-in-Aid from the Japan Society of the Promotion of Science (JSPS) (No. 19H00659) and CREST (JPMJCR15Q2) from the Japan Science and Technology Agency (JST). The synchrotron radiation experiment was performed with the approval of Photon Factory, KEK (2015G058). This work was supported by joint research program of ZAIKEN, Waseda University (Project No.31010).

---

[1] N. F. Mott, Philos. Mag. **6**, 287 (1961).

[2] D. Jérome, T. M. Rice, and W. Kohn, Phys. Rev. **158**, 462 (1967).

[3] J. Zittartz, Phys. Rev. **162**, 752 (1967).

[4] B. I. Halperin and T. M. Rice, Rev. Mod. Phys. **40**, 755 (1968).

[5] J. Neuenschwander and P. Wachter, Phys. Rev. B **41**, 12693 (1990).

[6] B. Bucher, P. Steiner, and P. Wachter, Phys. Rev. Lett. **67**, 2717 (1991).

[7] P. Wachter, B. Bucher, and J. Malar, Phys. Rev. B **69**, 094502 (2004).

[8] F. J. DiSalvo, D. E. Moncton, and J. V. Waszczak, Phys. Rev. B **14**, 4321 (1976).

[9] Th. Pillo, J. Hayoz, H. Berger, F. Lévy, L. Schlapbach, and P. Aebi, Phys. Rev. B **61**, 16213 (2000).

[10] D. Qian, D. Hsieh, L. Wray, E. Morosan, N. L. Wang, Y. Xia, R. J. Cava, and M. Z. Hasan, Phys. Rev. Lett. **98**, 117007 (2007).

[11] J. F. Zhao, H. W. Ou, G. Wu, B. P. Xie, Y. Zhang, D. W. Shen, J. Wei, L. X. Yang, J. K. Dong, M. Arita, H. Namatame, M. Taniguchi, X. H. Chen, and D. L. Feng, Phys. Rev. Lett. **99**, 146401 (2007).

[12] H. Cercellier, C. Monney, F. Clerc, C. Battaglia, L. Despont, M. G. Garnier, H. Beck, P. Aebi, L. Patthey, H. Berger, and L. Forró, Phys. Rev. Lett. **99**, 146403 (2007).

[13] C. Monney, H. Cercellier, F. Clerc, C. Battaglia, E. F. Schwier, C. Didiot, M. G. Garnier, H. Beck, P. Aebi, H. Berger, L. Forro, and L. Patthey, Phys. Rev. B **79**, 045116 (2009).

[14] C. Monney, E. F. Schwier, M. G. Garnier, N. Mariotti, C. Didiot, H. Beck, P. Aebi, H. Cercellier, J. Marcus, C. Battaglia, H. Berger, and A. N. Titov, Phys. Rev. B **81**, 155104 (2010).

[15] C. Monney, G. Monney, P. Aebi, and H. Beck, Phys. Rev. B **85**, 235150 (2012).

[16] C. Monney, G. Monney, P. Aebi, and H. Beck, New J. Phys, **14**, 075026 (2012).

[17] T. Rohwer, S. Hellmann, M. Wiesenmayer, C. Sohrt, A. Stange, B. Slomski, A. Carr, Y. Liu, L. M. Avila, M. Kalläne, S. Mathias, L. Kipp, K. Rossnagel, and M. Bauer, Nature **471**, 490 (2011).

[18] A. Kogar, M. S. Rak, S. Vig, A. A. Husain, F. Flicker, Y. I. Joe, Luc Venema, G. J. MacDougall, T. C. Chiang, E. Fradkin, J, van Wezel, P. Abbamonte, Science **358**, 1314 (2017).

[19] J. Kuneš and P. Augustinský, Phys. Rev. B 90, 235112 (2014).

[20] G. Khaliullin, Phys. Rev. Lett. **111**, 197201 (2013).

[21] S. A. Sunshine and J. A. Ibers, Inorg. Chem. **24**, 3611 (1985).

[22] F. J. DiSalvo, C. H. Chen, R. M. Fleming, J. V. Waszczak, R. G. Dunn, S. A. Sunshine, and J. A. Ibers, J. Less-Common Metals **116**, 51 (1986).

[23] Y. Wakisaka, T. Sudayama, K. Takubo, T. Mizokawa, M. Arita, H. Namatame, M. Taniguchi, N. Katayama, M. Nohara, and H. Takagi, Phys. Rev. Lett. **103**, 026402 (2009).

[24] Y. Wakisaka, T. Sudayama, K. Takubo, T. Mizokawa, N. L. Saini, M. Arita, H. Namatame, M. Taniguchi, N. Katayama, M. Nohara, and H. Takagi, J. Supercond. Nov. Magn. **25**, 1231 (2012).

[25] K. Seki, R. Eder, and Y. Ohta, Phys. Rev. B **84**, 245106 (2011).

[26] T. Kaneko, T. Toriyama, T. Konishi, and Y. Ohta, Phys. Rev. B **87**, 035121 (2013); Phys. Rev. B **87**, 199902(E) (2013).

[27] K. Seki, Y. Wakisaka, T. Kaneko, T. Toriyama, T. Konishi, T. Sudayama, N. L. Saini, M. Arita, H. Namatame, M. Taniguchi, N. Katayama, M. Nohara, H. Takagi, T. Mizokawa, and Y. Ohta, Phys. Rev. B **90**, 155116 (2014).

[28] Y. F. Lu, H. Kono, T. I. Larkin, A. W. Rost, T. Takayama, A. V. Boris, B. Keimer, and H. Takagi, Nature Commun. **8**, 14408 (2017).

[29] T. I. Larkin, A. N. Yaresko, D. Pröpper, K. A. Kikoin, Y. F. Lu, T. Takayama, Y.-L. Mathis, A. W. Rost, H. Takagi, B. Keimer, and A. V. Boris, Phys. Rev. B **95**, 195144 (2017).

[30] T. I. Larkin, R. D. Dawson, M. Höppner, T. Takayama, M. Isobe, Y.-L. Mathis, H. Takagi, B. Keimer, and A. V. Boris, Phys. Rev. B **98**, 125113 (2018).

[31] D. Werdehausen, T. Takayama, M. Höppner, G. Albrecht, A. W. Rost, Y. F. Lu, D. Manske, H. Takagi, and S. Kaiser, Sci. Adv. **4**, eaap8652 (2018).

[32] S. Mor, M. Herzog, J. Noack, N. Katayama, M. Nohara, H. Takagi, A. Trunschke, T. Mizokawa, C. Monney, and J. Stähler, Phys. Rev. B, **97**, 115154 (2018).

[33] S. Mor, M. Herzog, D. Golež, P. Werner, M. Eckstein, N. Katayama, M. Nohara, H. Takagi, T. Mizokawa, C. Monney, and J. Stähler, Phys. Rev. Lett. **119**, 086401 (2017).

[34] K. Okazaki, Y. Ogawa, T. Suzuki, T. Yamamoto, T. Someya, S. Michimae, M. Watanabe, Y. F. Lu, M. Nohara, H. Takagi, N. Katayama, H. Sawa, M. Fujisawa, T. Kanai, N. Ishii, J. Itatani, T. Mizokawa, and S. Shin, Nature Commun. **9**, 4322 (2018).

[35] K. Momma and F. Izumi, J. Appl. Crystallogr., **44**, 1272 (2011).

[36] J. Ghijsen, L. H. Tjeng, J. van Elp, H. Eskes, J. Westerink, G. A. Sawatzky, and M. T. Czyzyk, Phys. Rev. B **38**, 11322 (1988).

[37] K. Okada and A. Kotani, J. Phys. Soc. Jpn. **58**, 2578 (1989).

[38] K. Takubo, T. Mizokawa, J.-Y. Son, T. Nambu, S. Nakatsuji, and Y. Maeno, Phys. Rev. Lett. **99**, 037203 (2007).

[39] F. M. F. de Groot, J. C. Fuggle, B. T. Thole, and G. A. Sawatzky, Phys. Rev. B **42**, 5459 (1990).

[40] A. Fujimori, K. Mamiya, T. Mizokawa, T. Miyadai, T. Sekiguchi, H. Takahashi, N. Mori, and S. Suga, Phys. Rev. B **54**, 16329 (1996).

[41] T. Mizokawa, H. Namatame, A. Fujimori, K. Akeyama, H. Kondoh, H. Kuroda, and N. Kosugi, Phys. Rev. Lett. **67**, 1638 (1991).

Figure captions

Figure 1: (Color online) (a)Crystal structure of Ta_2NiS_5 created by VESTA[35], electronic configurations for Ni $3d^8$, $3d^9$, $3d^{10}$, Ta $5d^0$, $5d^1$, and the Brillouin zone of Ta_2NiS_5. The Ni chain and Ta double chain run along the a-axis. (b)ARPES spectra taken at 200 K for the entire valence band for Ta_2NiS_5 along a-axis with photon energy of 59 eV, along c-axis with photon energy of 59 eV, and along b-axis with photon energies from 57 eV to 69 eV.

Figure 2: (Color online) Upper panel: Ni $2p$ core-level spectra of Ta_2NiSe_5 (red circles) and Ta_2NiS_5 (blue triangles) and the calculated spectrum (solid curve) obtained by the cluster model calculation. Lower panel: Calculated line spectra without broadening which are decomposed into d^8, d^9L, and $d^{10}L^2$.

Figure 3: (Color online) (a)Ni $3p$-$3d$ resonant photoemission spectra for Ta_2NiS_5. The inset shows the photon energy dependence of the intensity at -5.5 eV. (b)Ni $3p$-$3d$ resonant photoemission spectra for Ta_2NiSs_5. The inset shows the photon energy dependence of the intensity at -5.0 eV.

Figure 4: (Color online) (a)Band dispersions and energy distribution curves taken at 200 K with photon energy of 65 eV for Ta_2NiS_5. The triangles and squares indicate band positions determined from energy and momentum distribution curves. (b) Band dispersions and energy distribution curves taken at 200 K with photon energy of 65 eV for Ta_2NiSe_5. (c) Band dispersions and energy distribution curves taken at 40 K with photon energy of 65 eV for Ta_2NiS_5.(d) Band dispersions and energy distribution curves taken at 40 K with photon energy of 65 eV for Ta_2NiSe_5.

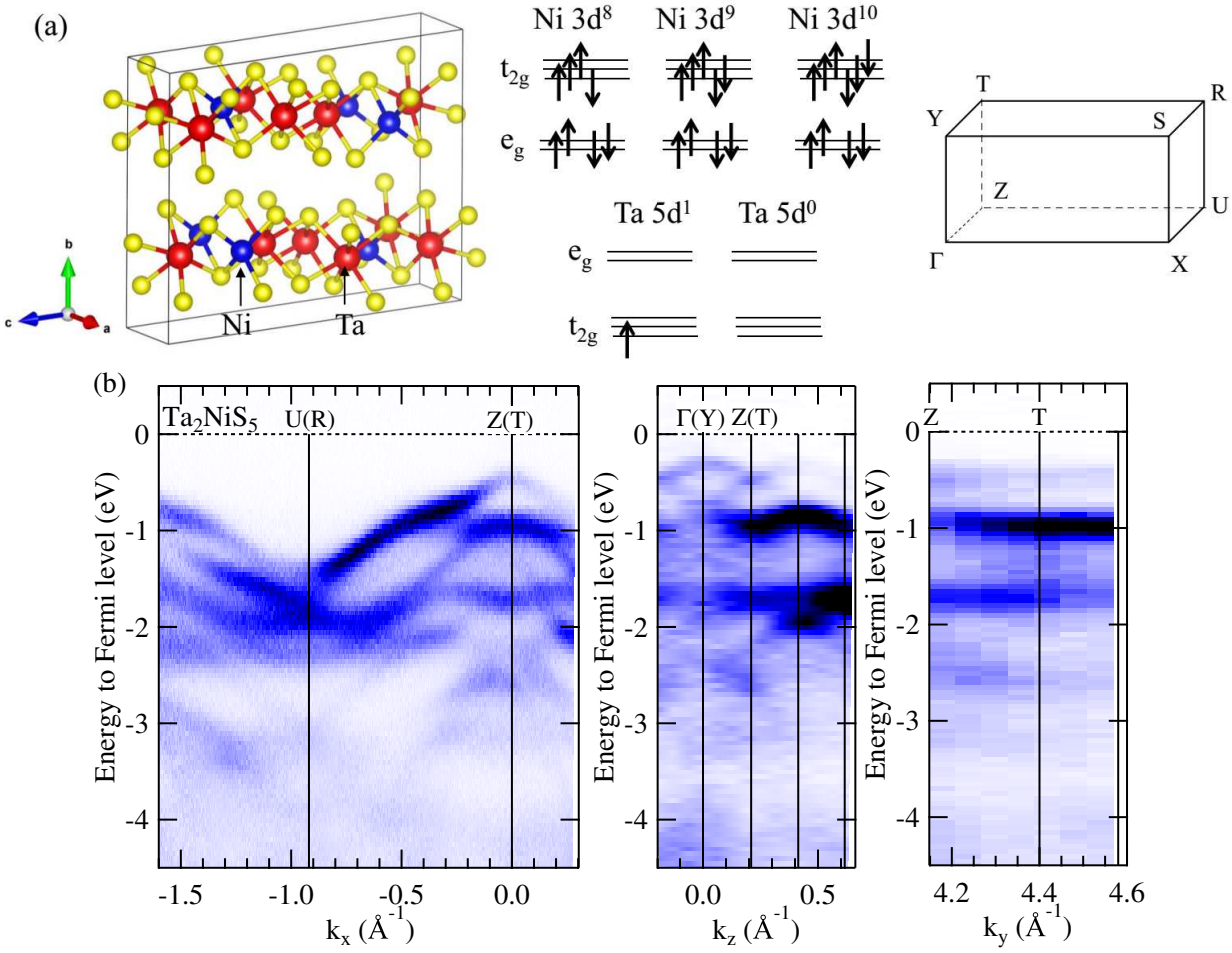

Figure 1 02Dec2019

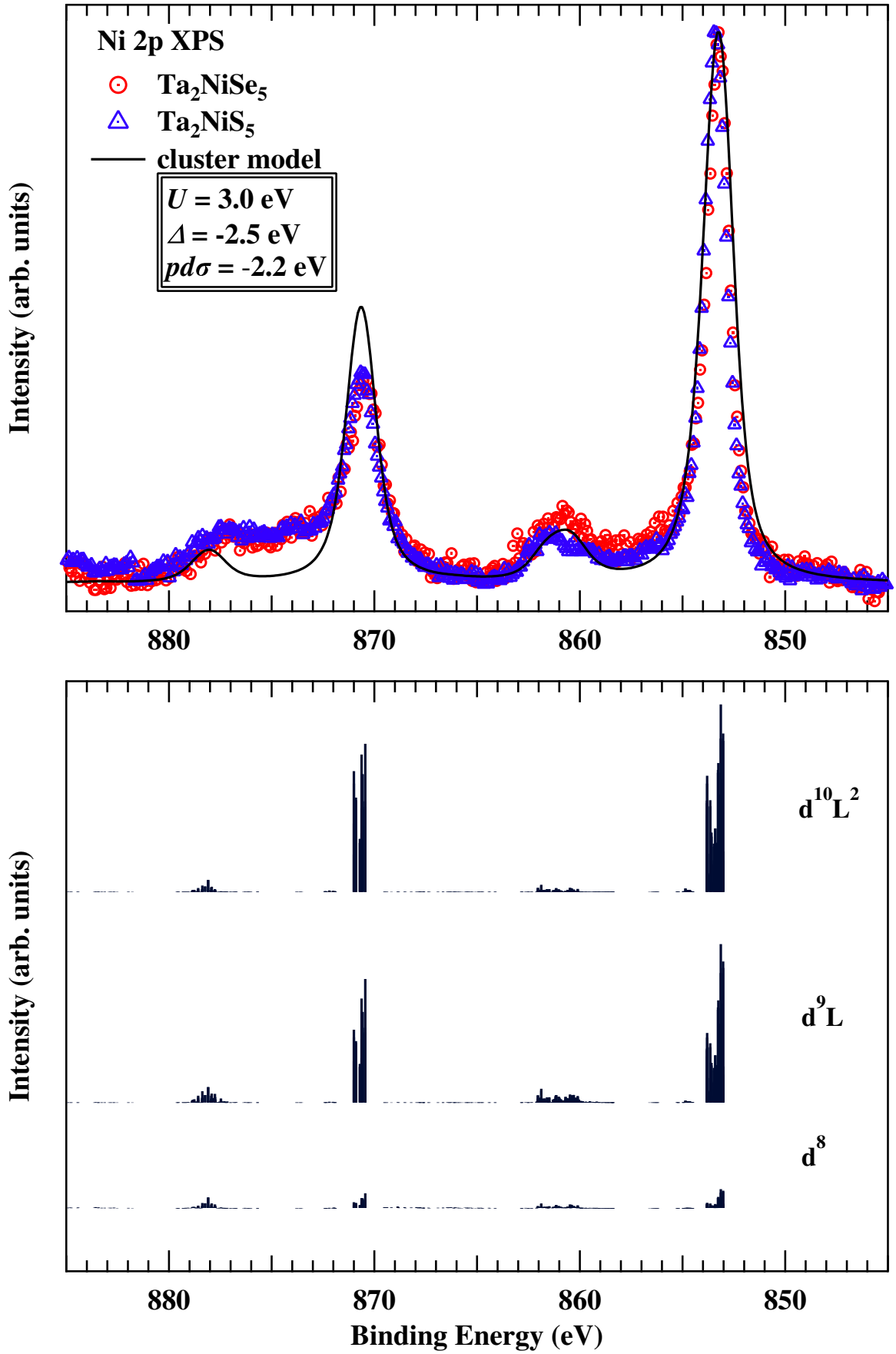

Figure 2 02Dec2019

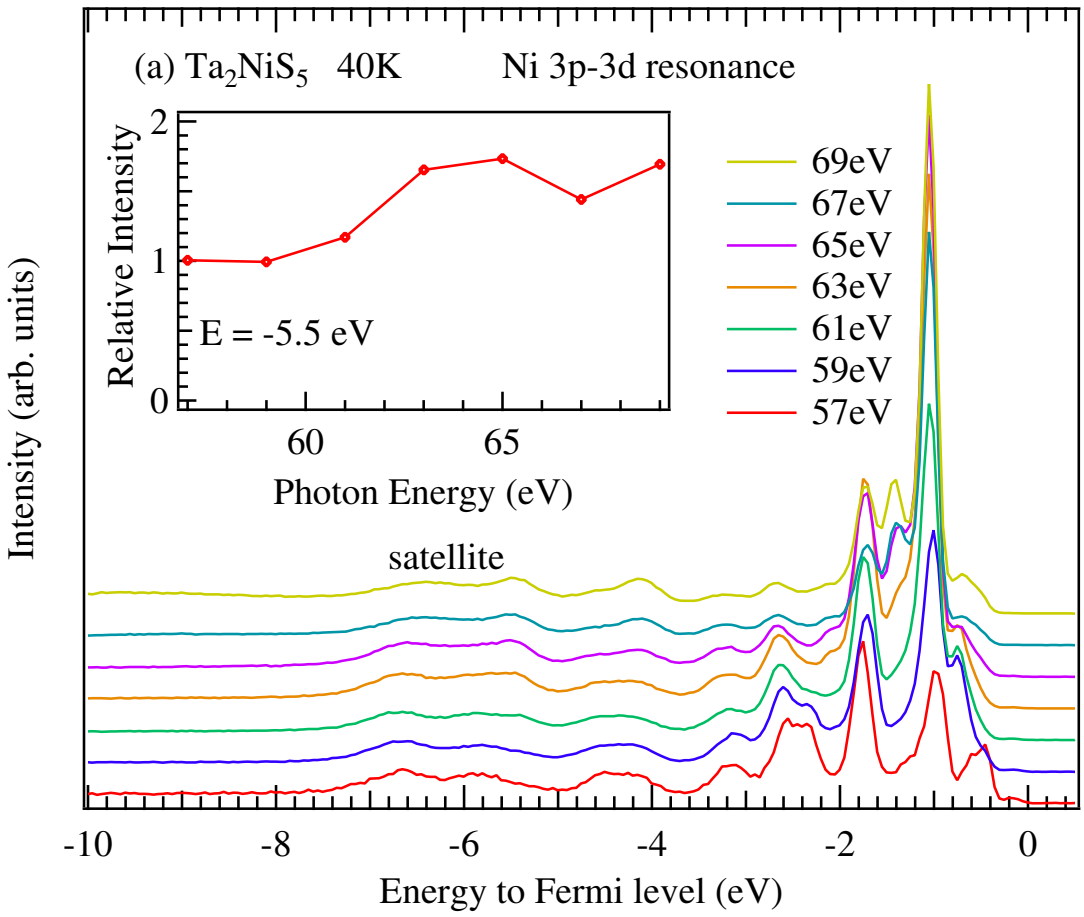

Figure 3a 02Dec2019

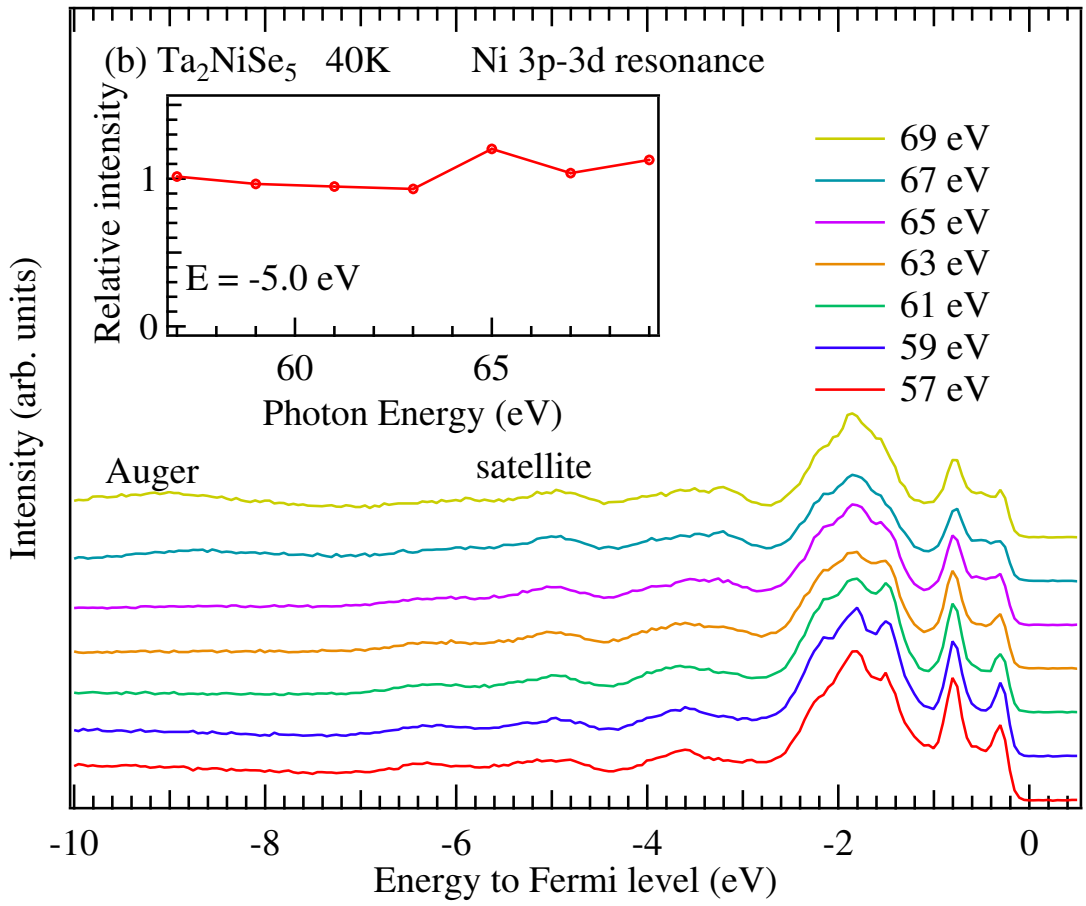

Figure 3b 02Dec2019

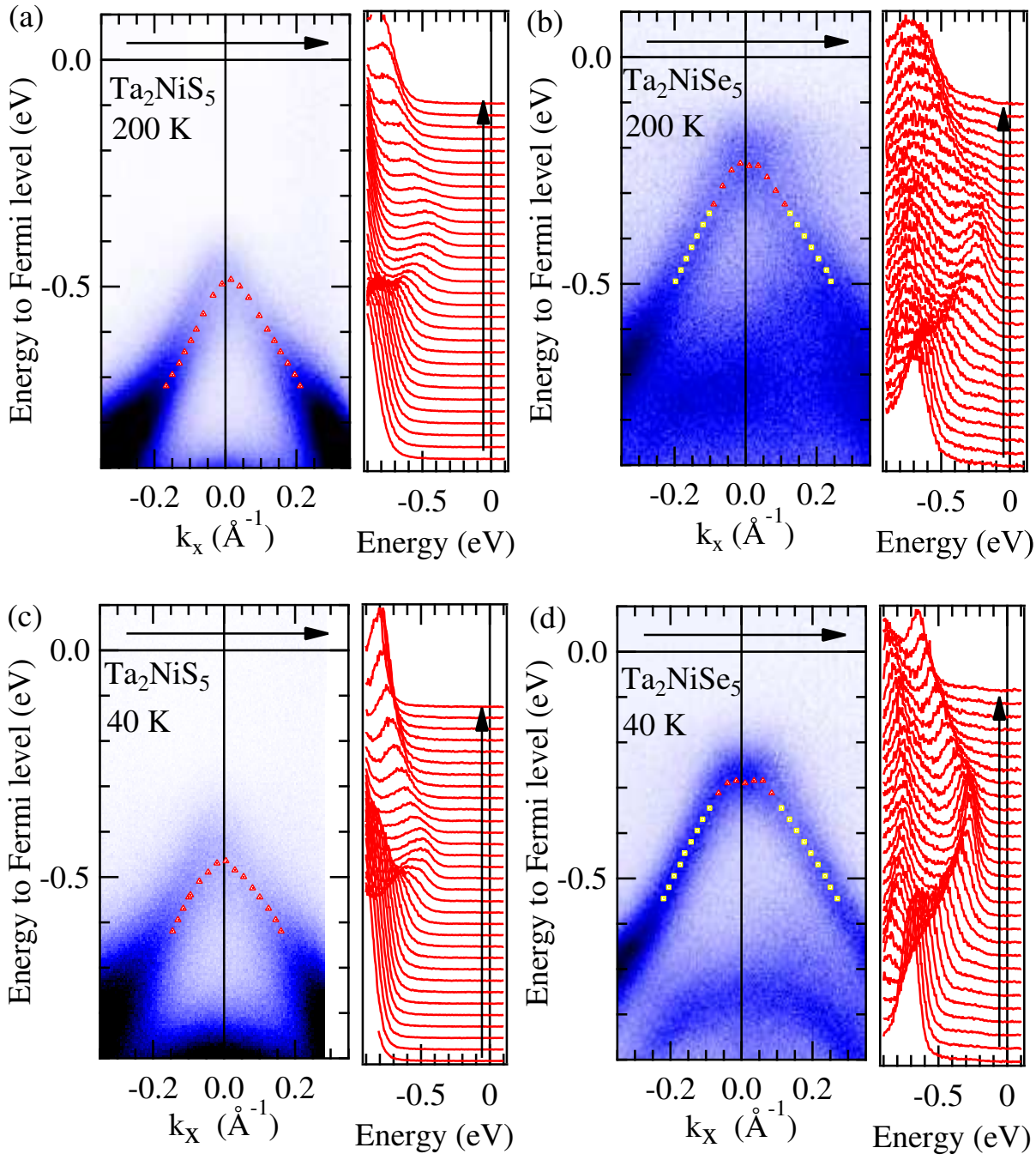

Figure 4 02Dec2019